*Int. J. Electrochem. Sci.*, 8 **(2013)** 10204 - 10218

International Journal of
ELECTROCHEMICAL
SCIENCE
www.electrochemsci.org

# Electro-Oxidation Activity of Pt-$CeO_x$ Carbon Supported Catalysts

*R. Fiala[1], I. Matolinova[1], V. Matolin[1,*], K. Sevcikova[1], H. Yoshikawa[2] and A. Tapan[3]*

[1] Charles University in Prague, Faculty of Mathematics and Physics, Department of Surface and Plasma Science, V Holešovičkách 2, 18000 Prague 8, Czech Republic
[2] Synchrotron X-ray Station at SPring-8, National Institute for Materials Science, Sayo, Hyogo 679-5148, Japan
[3] Gazi University, Department of Chemical Engineering, 06570, Maltepe, Ankara, Turkey
[*]E-mail: matolin@mbox.troja.mff.cuni.cz

*Received:* 30 May 2013 / *Accepted:* 16 June 2013 / *Published:* 1 August 2013

Platinum doped cerium oxide thin film catalyst reveals high activity at very low Pt content in proton exchange membrane fuel cells. The cyclic voltammetry study presented in this manuscript shows its electrochemical properties. Catalysts in form of very thin and highly porous layers deposited on carbon supports were prepared by magnetron sputtering. The sputtered catalysts were compared with the commercial Pt-C reference one. The photoelectron spectroscopy studies showed that the chemical state of platinum prepared by such a physical way is ionic which might be favorable for the catalytic activity. In this study the hydrogen and methanol electro oxidation was investigated using cyclic voltammetry. It was shown that the Pt-$CeO_2$ sputtered catalyst was more resistant to CO poisoning than the Pt-C reference.

**Keywords:** Proton exchange fuel cell catalyst, cyclic voltammetry, $CeO_2$, magnetron sputtering, graphite foil, gas diffusion layer

## 1. INTRODUCTION

Studies of the structure and properties of supported metal catalysts have found great interest in heterogeneous catalysis for many years. Noble metals dispersed on $CeO_2$ are widely used in automobile exhaust emission control due to oxygen storage capacity of ceria. Pt-oxide materials [1-3] have been reported as active catalysts for fuel cell applications. Recently, anode properties of Pt-$CeO_2$ have been investigated for the development of proton exchange membrane fuel cells (PEMFC) [4-9].

The catalysts are commonly prepared by wet techniques. Ionic Pt dispersed on a $CeO_2$ crystallite surface by the combustion method has been found to form active $Pt^{2+,4+}$ sites which led to high CO + NO and CO + $O_2$ reaction rates [10,11,12]. Pt ions incorporated in a $CeO_2$ matrix mostly in +2 oxidation state enhance hydrogen molecule dissociation to protonic hydrogen and increase hydrogen storage capacity of the catalyst [11,13].

It is surprising that enormous potential of well-developed thin film deposition and surface coating technology widely used in many fabrication processes was not largely utilized in catalysis yet. The main reason why application of thin film catalysts is aside the interest of chemists is that this technology is not suitable for massif large weight production in principle. The second reason is that the thin film coating is generally considered as a formation of compact low specific area surfaces. The coating process can be easily applied, however, for production of supported catalysts in case of fabrication of systems ranging from micrometers to several square meters (limitation being size of the deposition facilities), e.g. for production of fuel cells. The second drawback could be overcome by growing nanoporous catalyst film exhibiting large specific surface area [7,9,14].

In our previous works we showed that sputtered platinum doped cerium oxide based catalysts grown on the CNTs surface reveal very high catalytic activity when used as an anode in the proton exchange membrane fuel cell [9,14]. In this work we investigated carbon supported Pt doped cerium oxide thin film catalyst activity by using cyclic voltammetry (CV). The chemical and structural properties were investigated by electron microscopy and hard X-ray photoelectron spectroscopy.

## 2. EXPERIMENT

Two samples were investigated by cyclic voltammetry and hard X-ray photoelectron spectroscopy (HAXPES). The samples were prepared by non-reactive radio frequency (rf) magnetron sputtering deposition using composite Pt-$CeO_2$ target on two different substrates: Gas Diffusion Layer (GDL, Alfa Aesar, Toray carbon paper, TGP-60) and graphite foil (GF, Alfa Aesar, 0.254 mm thick). Composite target was prepared by placing 2 pieces of 0.5 mm thick and 10 mm long Pt wire on the 2" ceria target surface in the radial direction. The rf sputtering was performed at a distance of 90 mm from the GDL substrate using rf power of 100 W giving a growth rate of the films of 2 nm $min^{-1}$. The growth rate was calibrated by checking the reference film cross view by SEM and the film thickness was determined from time of the deposition. The deposition was carried out at room temperature of the substrate in an Ar atmosphere by keeping the total pressure in the deposition chamber constant at $4 \times 10^{-1}$ Pa. The method is currently called "non-reactive sputtering" because only Ar is introduced into the chamber; however oxygen was released from the oxide target by the sputtering process which ensured oxidation of the Ce atoms sputtered off the target.

Morphology of Pt-$CeO_2$/GDL and Pt-$CeO_2$/GF was observed by means of scanning electron microscopy (SEM) by using a TESCAN - MIRA microscope at 30 keV electron beam energy.

Graphite foil (GF, Alfa Aesar, 0.254 mm thick) was used as a second catalyst substrate. Roughness of the graphite foil surface was checked by Atomic Force Microsopy (AFM) (not shown).

It revealed layered flat surface with wide shallow craters. The depth of the craters was estimated to be of 2 nm and roughness of 0.5 nm, in average.

The HAXPES measurements were performed at the undulator beamline BL15XU of the SPring-8 synchrotron light source. The X-ray was monochromatized at 5950.2 eV by using a Si 333 channel-cut post-monochromator with the total energy resolution of 280 meV. All HAXPES experiments were performed ex situ in ultra-high vacuum (UHV) experimental chamber operating at base pressures around $5 \times 10^{-9}$ mbar, the spectra were taken at the grazing photon incidence and normal emission geometry.

Pt concentration was determined by means of a laboratory XPS using Al Kα 1486.61 eV excitation and the thickness of layer was obtained by observing the breakage of the layer using a scanning electron microscope. The thickness of layers were 30 nm, approximately.

Cyclic voltammetry was performed on a three-electrode system that consists of a saturated calomel reference electrode (SCE), glassy carbon disc working electrode and platinum wire counter electrode. Cell potential was controlled by a potentiostat (AFBP1, Pine Inst.) that was connected to a PC. Glassy carbon working electrode with an area of 0.256 $cm^2$ was loaded with the reference catalyst powder (Pt-C nanopowder or loaded with the graphite foil or with the GDL both coated by Pt-$CeO_2$ sputtered layer. Loading on the glassy carbon disc was done after 10 μl injection of 5wt% Nafion solution on the electrode surface. During cyclic voltammetry, the working electrode was scanned at a rate of 10 mV/sec and 100 mV/sec in 0.5M $H_2SO_4$ and 0.5M $H_2SO_4$ + 0.5M $CH_3OH$ electrolyte environments. Potentials recorded during cyclic voltammetry were converted with respect to the standard hydrogen electrode (NHE).

Hydrogen and methanol electro-oxidation activities were investigated on Pt-$CeO_2$ deposited on carbon gas diffusion layer (GDL) and graphite foil (CF) by magnetron sputtering technique. Sputtered Pt-$CeO_2$ layer activities were compared with that of the Pt-C (platinum black 40at% Pt, Alfa Aesar) nanopowders.

In order to determine methanol electro-oxidation activity, voltammograms obtained in 0.5 M $H_2SO_4$ base electrolyte were compared with those obtained in 0.5M $H_2SO_4$+ 0.5M $CH_3OH$ solution. In case of hydrogen electro-oxidation, cyclic voltammetric experiments were performed in the base electrolyte and in the base electrolyte during and after hydrogen bubbling at a flow rate of 10 ml/min. All cyclic voltammetric experiments were performed only after conditioning catalyst coated electrode at 0 V for 10 seconds. After application of magnetron sputtering technique, catalyst coated electrode were directly tested by cyclic voltammetry without any further pre-activation step.

## 3. RESULTS

The surface of GDL and CF coated by Pt-$CeO_2$ were investigated by electron microscopy. SEM images show a high porosity for both kinds of substrates which is given by growth of catalyst islands that have fractal like structure (see Fig. 1). The size of these islands was obtained by software GWIDDION giving the islands lateral average size of 14 nm.

Concentration of Pt was determined from XPS experiment by using tabulated sensitivity factors. The atomic concentration ratio Pt/Ce for sputtered layer on GDL and on CF was 0.1, which corresponded to loading of 2 μg(Pt)/cm$^2$, respectively.

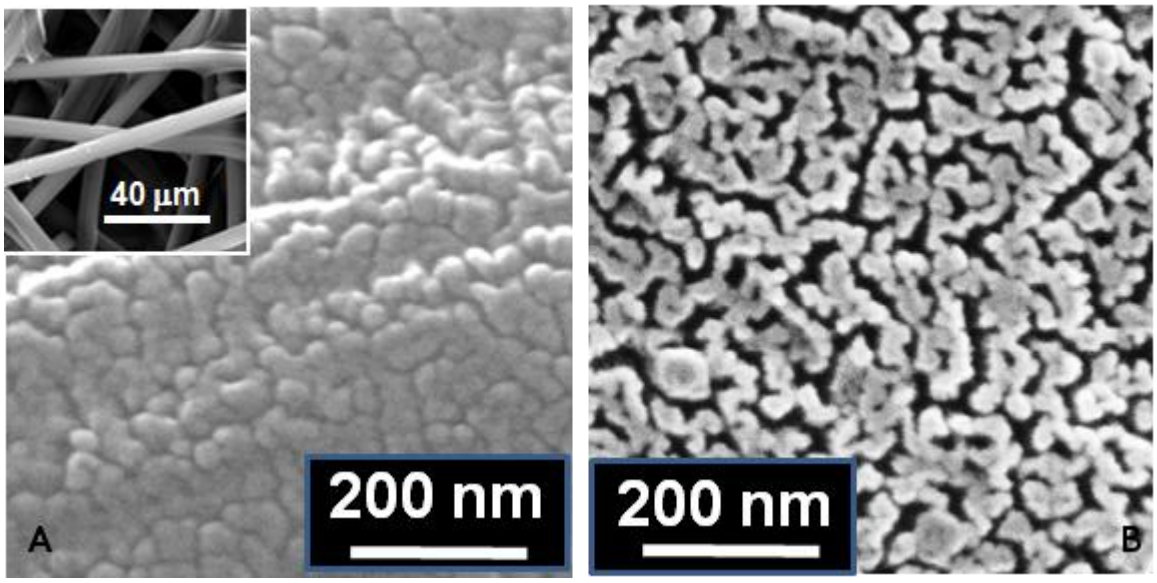


**Figure 1.** The SEM images of the coated GDL (a) and coated graphite foil (b).

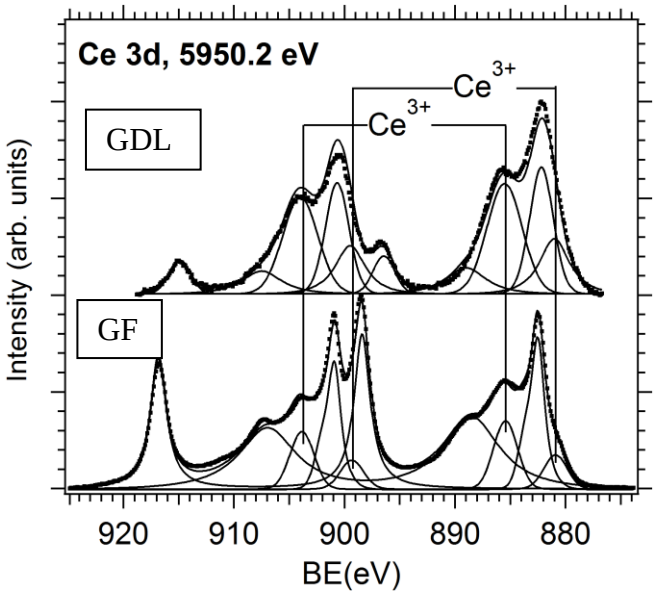


**Figure 2.** Ce 3d HAXPES spectra measured on the sputtered Pt-$CeO_2$ layer on the GDL (up) and on GF (bottom). The fits of the spectra with $Ce^{3+}$ and $Ce^{4+}$ states are shown. Photon energy: 5950.2 eV.

The HAXPES technique is suitable for porous structure studies due to its large information depth of analysis. For example the kinetic energy of Ce 3d photoelectrons excited by 5950.2 eV photons was about 5.1 keV corresponding to an inelastic mean free path (λ) in $CeO_2$ about 7 nm [14].

Such a large inelastic mean free path allows us to take information from the depth up to 21 nm because about 95% of the photoelectron signal comes from the surface layer 3 λ thick.

In Fig. 2 we show Ce 3d HAXPES spectra obtained for both samples. It consists of three $3d_{5/2}$-$3d_{3/2}$ spin-orbit-split doublets characteristic of $Ce^{4+}$ states [16] and two $3d_{5/2}$-$3d_{3/2}$ spin-orbit-split doublets characteristic of $Ce^{3+}$ states at 885.6 and 881.1 eV. The doublets represent different 4f configurations in the photoemission final state and arise from the Ce 4f hybridization in both the initial and the final states [17]. The Ce $3d_{5/2}$ $4f^2$ peak at 883 eV is fitted by an asymmetric feature accordingly to [18]. Fig. 2 shows that cerium oxide is partially reduced which was found to by characteristic for porous cerium oxide sputtered on carbon substrates. The Ce ratio concentrations $Ce^{3+}/Ce^{4+}$ determined from the HAXPES spectra by using areas of corresponding elemental peaks are 0.21 and 1.15 for catalysts supported by the GF and GDL, respectively.

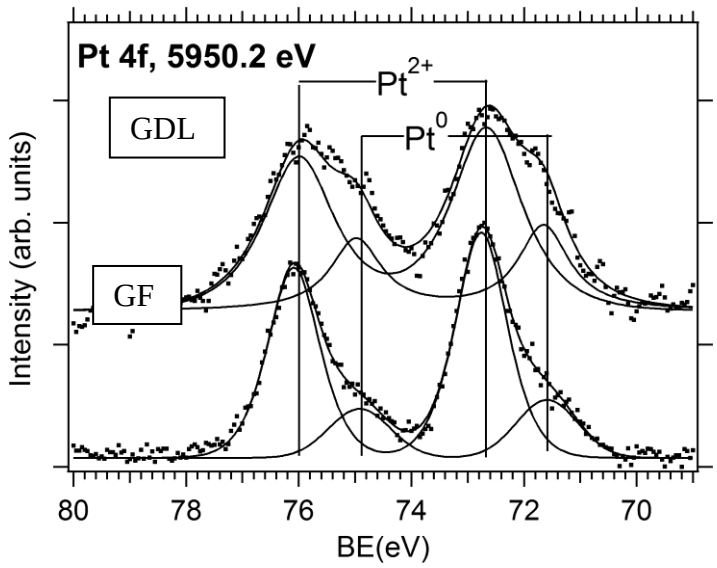


**Figure 3.** Pt 4f HAXPES spectra measured on the sputtered Pt-$CeO_2$ layer on the GDL (up) and on GF (bottom). Fits show metallic and Pt and $Pt^{2+}$ ionic component. Photon energy: 5950.2 eV.

The Pt 4f HAXPES spectra obtained for the Pt-doped ceria films are plotted in Fig. 3. The spectra reveal Pt $4f_{7/2}$-$4f_{5/2}$ doublets at energies 72.6-75.9 eV and 71.5-74.8 eV, respectively. The first one can be associated with $Pt^{2+}$ content [19] whilst the second corresponds to $Pt^0$. In case of the GDL substrate, the $Pt^{2+}/Pt^0$ ratio is smaller than that of the GF.

By summarizing results concerning chemical states of sputtered platinum doped ceria layers on GDL and GF, we can see that layer on the GF contains higher relative content of ionic platinum comparing that one on the GDL. By comparing cerium oxide chemical states of these samples we can see that higher concentration of ionic Pt is characteristic for more stoichiometric cerium oxide whilst ceria reduction is connected to an increase of metallic Pt content.

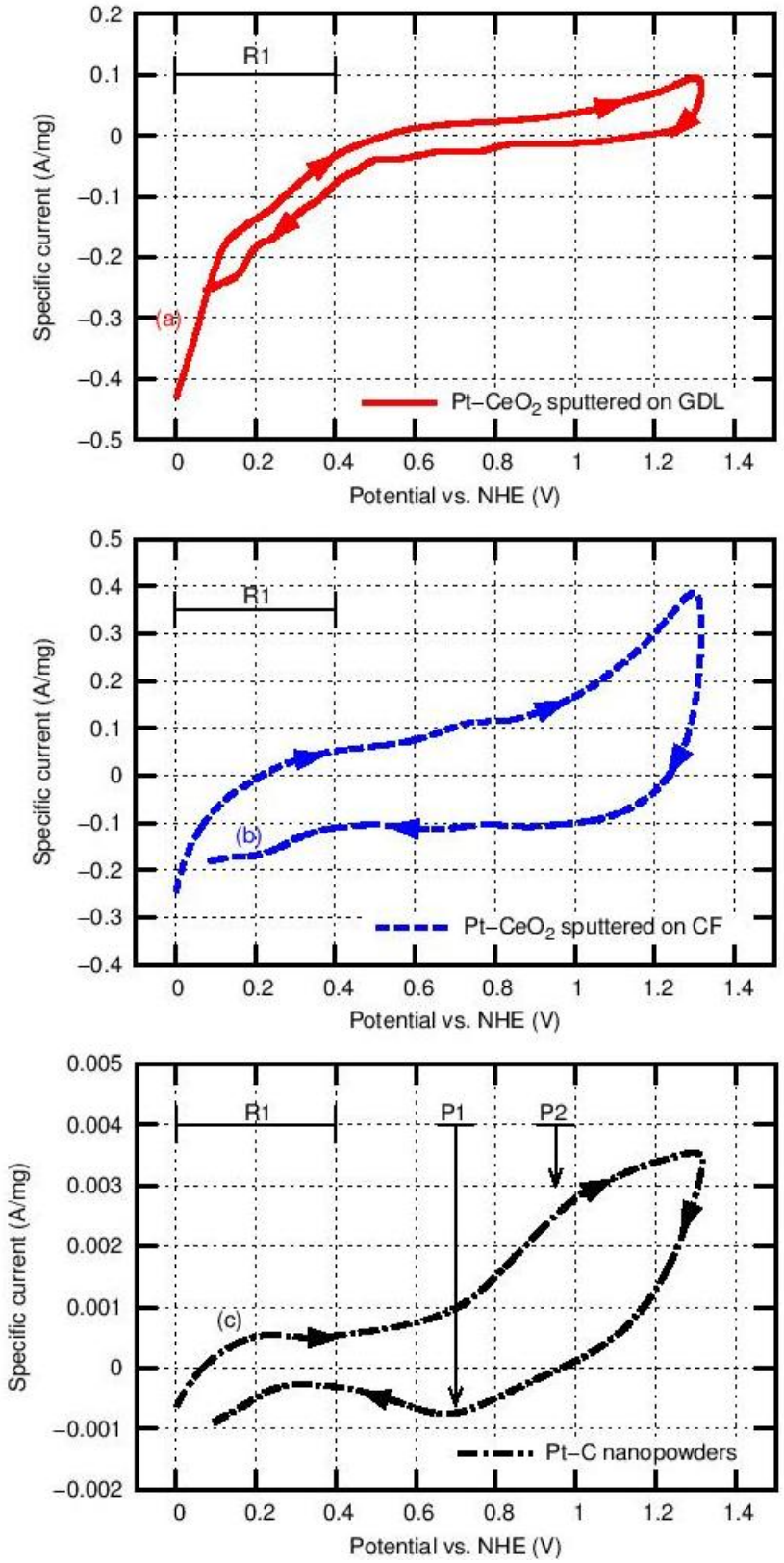


**Figure 4**. The voltammograms of Pt-$CeO_2$ sputtered on the gas diffusion layer (a), on the graphite foil (b), Pt-C nanopowder (c) in the 0.5 M $H_2SO_4$ solution at a scan rate of 10 mV/s.

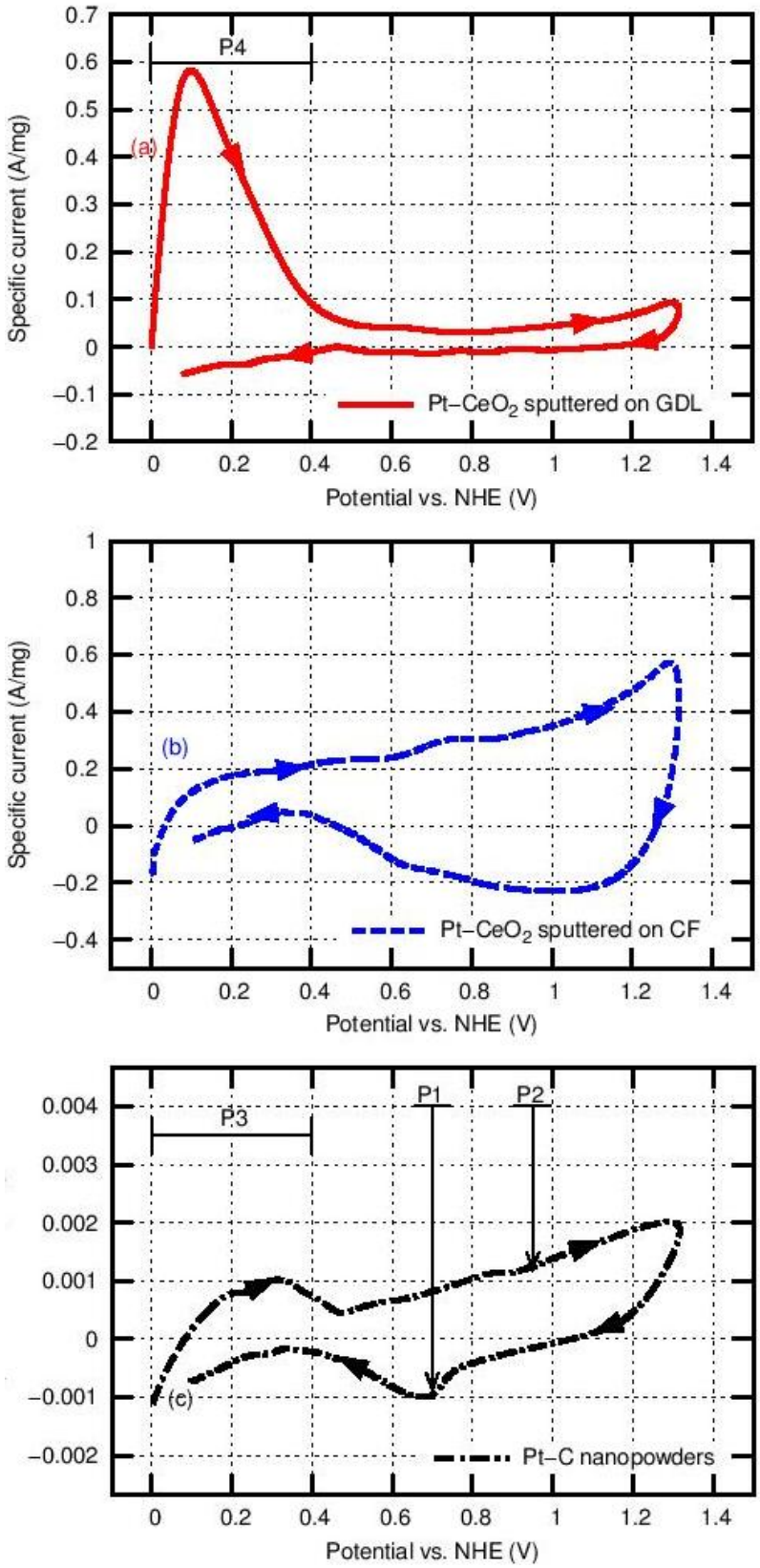


**Figure 5.** The voltammograms of Pt-$CeO_2$ sputtered on the gas diffusion layer (a), on the graphite foil (b), Pt-C nanopowder (c) in 0.5 M $H_2SO_4$ solution at a scan rate of 10 mV/s during hydrogen bubbling. Hydrogen was bubbled at a rate of 10 mL/min.

Voltammograms obtained in 0.5 M H2SO4 solution for commercial Pt-C nanopowder and Pt-CeO2 catalyst film sputtered on the GDL and GF can be seen in Figs. 4, 5 and 6. In case of base electrolyte (Fig. 4) shapes of voltammograms are mostly comparable except the 0-0.4 V potential range (R1). The difference in 0-0.4 V potential range is assumed to be due to very high hydrogen evolution rate on Pt-CeO2 on the GDL. In case of Pt-C, there are small features at 0.7 V and close to 0.95 V (P1 and P2 in Fig. 4), which were similar to those observed for mesoporous Pt [20] and in other previous works [21-24]. In addition, although voltammograms were nearly featureless, the current activities of Pt-CeO2 sputtered electrodes in 0.6 - 1.2 V potential range (where PtO formation, O2 evolution and reduction of oxide take place) were higher than that of the Pt-C nanopowders (for GDL 50 times and for GF 100 times). The high current activities prove higher electrochemical activity.

During the hydrogen bubbling in the base electrolyte (Fig. 5) no appreciable change in the features of Pt-C nanopowder were observed compared to base electrolyte (Fig. 4) voltammogram. The hydrogen adsorption-desorption peaks in the region 0.0 – 0.4 V were distinctive (see oxidation peak *P3*) and the oxidation reduction peaks *P2* and *P1* were visible as well. However, the current activity obtained for sputtered layer on CF increased (300 times higher relative to the Pt-C reference). In addition, an oxidation peak between 0.0-0.4V (*P4*) was also observed on Pt-$CeO_2$/GDL (top plot in Fig. 5). The oxidation peaks were assumed to be due to the hydrogen desorption from the platinum surface which can be explained by the electrochemical reactions described by Eqs 1 and 2:

$^{(1)}$ $Pt + H_2 \rightarrow Pt + 2\,H^+ + 2\,e^-$

$^{(2a)}$ $2\,Pt^{n+} + H_2 \rightarrow 2\,Pt^{(n-1)+} + 2\,H^+$

$^{(2b)}$ $2\,Pt^{(n-1)+} + 2\,H^+ \rightarrow 2\,Pt^{n+} + 2\,H^+ + 2\,e^-$ .

The equation 1 describes hydrogen adsorption/desorption in case of the Pt-C nanopowder and partially in case of Pt-$CeO_2$ partially containing metallic platinum and the equation 2a and 2b describe Pt-$CeO_2$/GDL and Pt-$CeO_2$/CF containing ionic platinum (shown by HAXPES studies) Although, these equation (2a,2b) illustrate the real mechanism in simplified way. The oxidation mechanism determined for Pt-$CeO_2$ sputtered catalyst is more discussed in discussion part. The oxidation peak was not observed on Pt-$CeO_2$/GF in comparison with the same at Pt-$CeO_2$/GDL in the region 0.0 – 0.4 V. It can be explained by higher contents of ionic Pt and $Ce^{4+}$. In case of Pt-$CeO_2$/GF the content of $Ce^{4+}$ is 5.5 times higher than in case of Pt-$CeO_2$/GDL, which means that the platinum ionic behaviors is more significant for Pt-$CeO_2$/CF and also the schemas 2a and 2b are more significant for it.

The difference between the voltammograms of Pt-$CeO_2$ on GDL and GF indicates different hydrogen oxidation activity. It can be explained by substantially different structure of both layers or by different ratios of $Pt^{2+}/Pt^0$ as presented in the discussion part.

In order to confirm this hypothesis, hydrogen bubbling was stopped after one cycle and the change in the peak features on Pt-$CeO_2$/GDL was observed as can be seen in Fig. 6_During cycling when hydrogen was stopped, the oxidation peak *P4* on Pt-$CeO_2$/GDL between 0.0-0.4V lost its current activity (cycle by cycle) and after the first scan a hydrogen adsorption-desorption peaks which are typical for Pt crystalline surface were formed. In case of Pt-$CeO_2$/GF, no oxidation peak feature was observed but there is evident a high double layer capacitance (in anodic part 0.40-0.80 V and 0.65-0.40 in cathodic part) which may be caused by hydrogen adsorption on the surface.

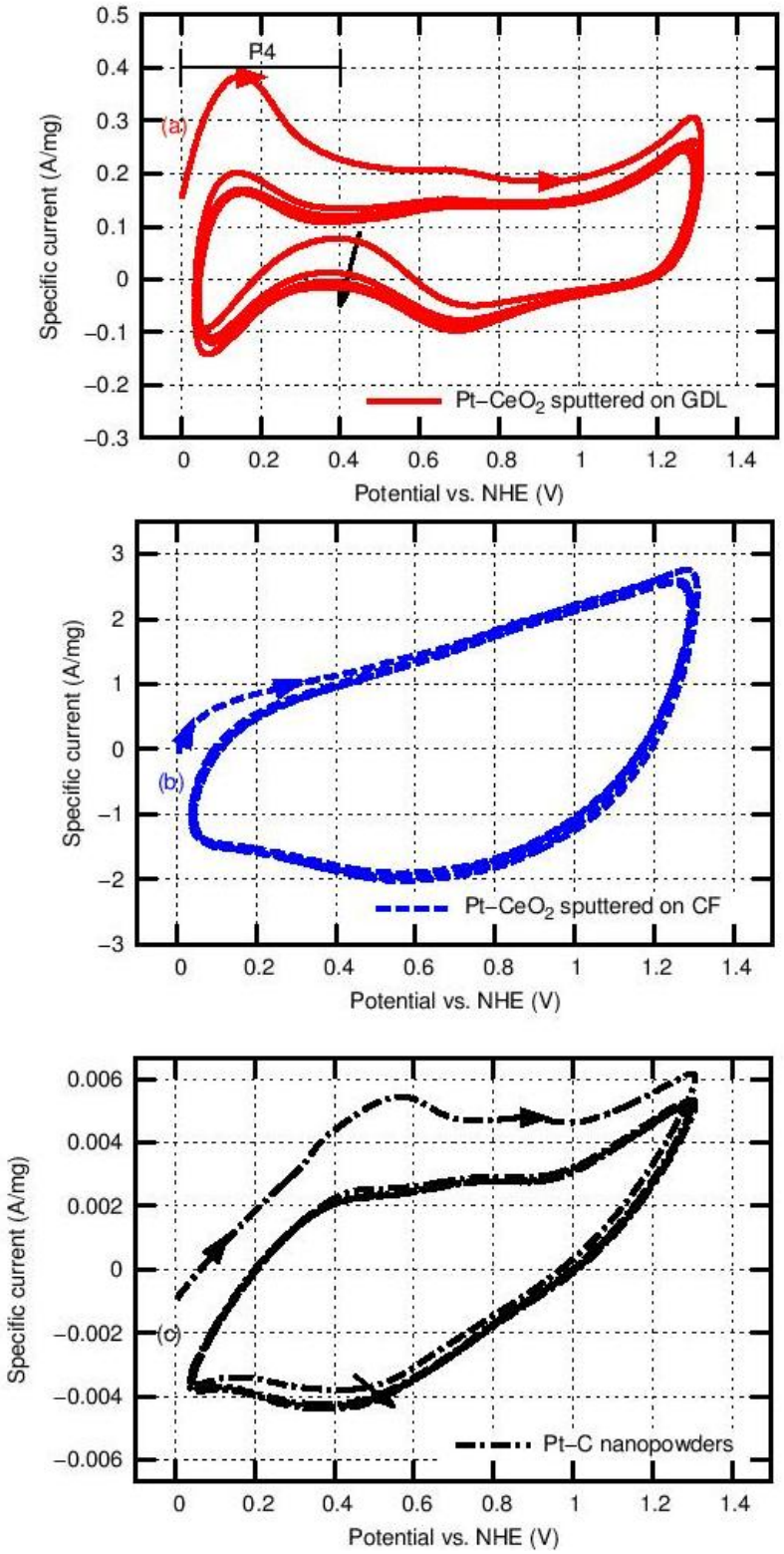


**Figure 6.** The voltammograms of Pt-$CeO_2$ sputtered on the gas diffusion layer (a), on the graphite foil (b), Pt-C nanopowder (c) during 10 cycles at a scan rate of 100 mV/s in 0.5 M $H_2SO_4$ solution after hydrogen bubbling.

This high double layer capacitance and high double layer capacitance in case of GDL relative to the Pt-C reference confirmed the high porosity showed by using scanning electron microscope (see above).

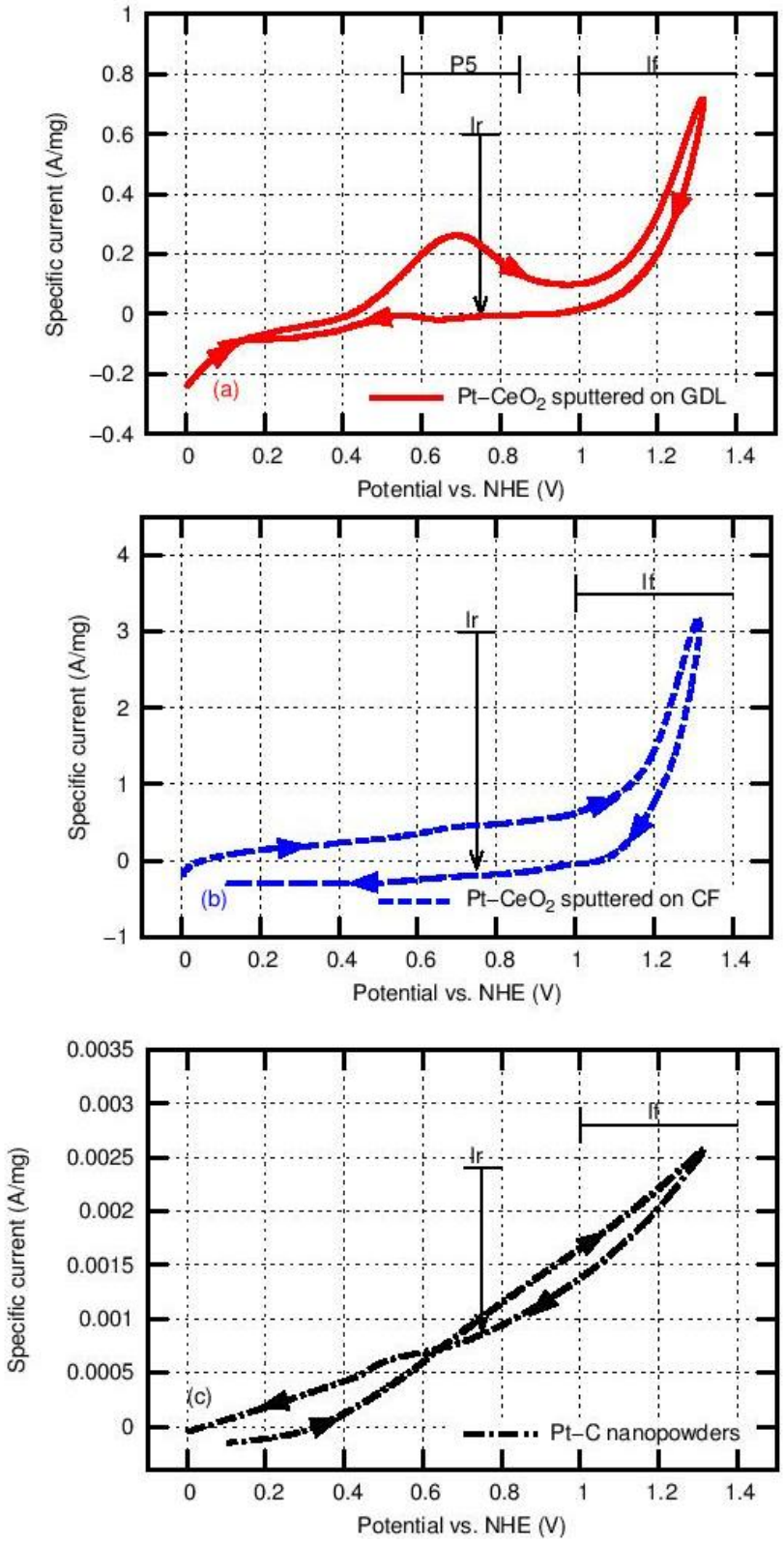


**Figure 7.** The voltammograms of Pt-$CeO_2$ sputtered on the gas diffusion layer (a), on the graphite foil (b), Pt-C nanopowder (c) in 0.5 M $H_2SO_4$ + 0.5 M $CH_3OH$ solution at a scan rate 10 mV/s.

In order to investigate methanol oxidation properties of the Pt-C nanopowders and Pt-$CeO_2$ thin films sputtered on the GDL and GF, cyclic voltammetry was also performed in 0.5M $CH_3OH$ + 0.5M $H_2SO_4$ electrolyte. Voltammograms can be seen in Fig. 7. Methanol electro-oxidation properties of the

Pt-C nanopowder was similar to those obtained in previous studies [22,24,25]. Methanol electro-oxidation seems to start at about 0.3 – 0.4 V on Pt-C, which is in agreement with [21,26-28]. The comparison of voltammograms of nanopowders and Pt-$CeO_2$ sputtered layers indicated that the gap of 1.2 V between current activities of the Pt-C nanopowder and sputtered layers dramatically increased in the 0.5M $CH_3OH$ + 0.5M $H_2SO_4$ electrolyte (600 times higher for GF and 200 times higher for GDL relative to the Pt-C nanopowders). The increase of current activities at 1.2V on sputtered layers is assumed to be due to the enhancement of direct methanol oxidation to carbon dioxide. In addition, completely different voltammograms were observed in case of nanopowders and sputtered layers which indicated different methanol electro-oxidation mechanisms. During cyclic voltammetry of Pt-$CeO_2$ sputtered on the GF and GDL in the 0.5M $CH_3OH$ + 0.5M $H_2SO_4$ electrolyte (see Fig. 7), an oxidation peak feature were detected for both GF and GDL close to 1V (*If*) and another oxidation peak was detected at 0.7 V *(P5)* for the GDL during the forward scan. By comparing data with literature, we can see that CV obtained for sputtered Pt-$CeO_2$ on GF (Fig. 7 (b)) are very similar to the CV result obtained by S. Sharma et al. [29], where the authors investigated catalyst $Ce_{0.98}Pt_{0.02}O_{2-\square}$ prepared by solution combustion method.

Origin of the *P5* peak is unclear as well as the peak intensity difference by comparing GDL and CF supported catalysts films.

## 4. DISCUSSION

Recently, we have shown that porous growth of cerium oxide thin films deposited by magnetron sputtering is typical for the CNT substrate [9]. However, comparing the growth on different carbon substrates (HOPG, glassy carbon) including GDL and graphite foil (GF), (see this work), we found that formation of porous ceria structures is a general property resulting from a magnetron plasma etching of carbon substrates. It can be well seen in Fig. 1 where SEM images of the catalyst coated GDL and graphite foil are presented. The average diameters of the largest grain are comparable in both cases. However, the total active surface area is not known because the grains very probably exhibit nanoporous structure themselves. In order to elucidate this point, surface area evaluation using a desorption technique should be performed in further studies. Furthermore, in the case of the GDL the catalyst layers reveal variable structure going from the top part the most exposed to the deposition flux (maximum thickness) through lateral (very thin) to rear (unexposed) part of the GDL fibers (fibers are shown in Fig. 1 inset). It results in variable thickness of the films deposited on the GDL as it is schematized in Fig. 8. Therefore any sound discussion of structure and morphology determining the catalyst properties are not, in the case of the GDL supported films, relevant. In contrary the invariable character of the GF supported catalyst film over the whole substrate makes this sample suitable for fundamental study of the reaction mechanism.

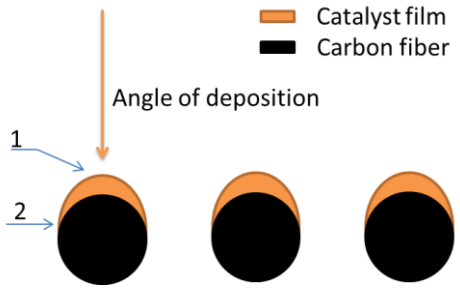


**Figure 8**. Thickness of catalyst coating of the GDL fibers. 1 – The layer of nominal thickness; 2 – region of variable low thickness.

In order to study hydrogen oxidation on the catalysts we performed CV with hydrogen bubbling. Fig. 5 shows that voltammograms obtained for both samples, Pt-$CeO_2$/GDL and Pt-$CeO_2$/GF were similar contrary to the hydrogen desorption peak *P4* which appeared only on Pt-$CeO_2$/GDL between 0.0-0.4 V. The origin of this desorption feature was not clear; however it might be explained as a result of non-homogenous structure and variable layer thickness of sputtered film on GDL. In literature, the same sharp peak was reported by Wu et al. [21] and Iwasita et. al. [30] on PtRu/C catalyst prepared via reduction by $H_2$. It might be possible that this peak is connected to metallic Pt which is shown by the HAXPES (see Fig. 3). The oxidation reduction peaks *P3* at 0.95 V and *P2* at 0.7 V, characteristics of polycrystalline Pt, were not detected on sputtered catalyst. This can be explained by the partial coverage of Pt surface by ceria layer, inhibiting oxidation of Pt as observed before by Fugane et al. [22].

During cyclic voltammetry, when hydrogen bubbling was stopped (Fig. 6), the high oxidation peak feature *P4* at 0.0-0.4 V disappeared and the peaks typical for Pt crystalline surface appeared (can be compared with [20,21,31,32]). Emergence of these peaks in case of the GDL may be due to the higher amount of metallic Pt in the sputtered GDL layer compared to the GF layer.

After $H_2$ bubbling was stopped (Fig. 6) we can see the effect of double layer capacitance for both GF and GDL supported catalysts. However it is seen that the double layer capacitance was much higher on the graphite foil which typically indicated higher electrochemical surface area. This may be due to the activation of highly porous structure after reduction of the oxides by hydrogen leading to the removal of dielectric layer and this effect was more significant in case GF. Moreover, the reduction by hydrogen can cause increase of porosity of oxide films in general. This phenomenon is more likely to occur when Pt-$CeO_2$ sputtering technique is used. In addition, this high double layer capacitance revealing only peaks of adsorptions and desorptions may indicate that most of Pt in sputtered layer on GF and on the GDL was covered by a cerium oxide layer, which is in agreement with the same statement in [22]. High double layer capacitance after hydrogen bubbling was also observed on Pt-C nano powder, nevertheless it was not as high as on GF and GDL coated by sputtered layer. However the suppressed hydrogen desorption and oxide reduction peaks were still slightly visible during several scans of cyclic voltammetry.

An important conclusions that can be drawn from the above results are that Pt-$CeO_2$ catalysts sputtered on the GDL and GF exhibit superior performance for hydrogen oxidation compared to the

commercial Pt-C nanopowder (i) and hydrogen oxidation behavior of the catalyst strongly depends on type of the carbon substrate (GDL or GF) (ii). This conclusion is in agreement with results of our previous fuel cell test [9,14] of Pt-$CeO_2$ catalysts deposited on the CNTs.

As it has been shown above, during cyclic voltammetry of Pt-$CeO_2$ sputtered on the GF and GDL in the 0.5M $CH_3OH$ + 0.5M $H_2SO_4$ electrolyte (see Fig. 7), an oxidation peak was detected for both GF and GDL close to 1V (*If )* and another oxidation peak was detected at 0.7 V *(P5)* for the GDL during the forward scan. In the literature, it is reported that two specific peaks can be seen during methanol electro oxidation. They are methanol oxidation peak (*If*) close to 1 V appearing during the forward scan and attributed to the formation of $CO_2$, and an oxidation peak close to 750 mV attributed to removal of incompletely oxidized carbonaceous species (*Ir*) formed during the forward scan [26, 29,32-35]. It was also noted in literature that a high intensity ratio of the forward peak (*If*) to the reverse peak (*Ir*) signify that the catalyst reveals a high CO tolerance and low accumulation of carbonaceous species on the catalyst surface. Voltammograms of sputtered Pt-$CeO_2$ layers in Fig. 7 show that the reverse scan is almost flat for both, coated GDL and GF while in the forward scan an anodic peak ($I_f$) giving very high $I_f/Ir$ ratio is seen. The high $I_f/Ir$ ratio indicates that sputtered GDL and CF exhibit very high CO tolerance compared to the commercial Pt-C nanopowder. We should note that a CO tolerance of Pt-$CeO_2$ in form of powder was also reported in literature [26,34], where the $I_f/I_r$ ratio was close to one. By comparing with the Pt-$CeO_2$ catalyst powder, the high CO tolerance of sputtered Pt-$CeO_2$ can be explained by the presence of ionic platinum and ceria since both of them have lower activity than metallic Pt for CO adsorption and so higher resistance against CO poisoning as reported by Sharma et al. [29], where author present an increase of CO tolerance for Pt-$CeO_2$ catalyst prepared by combustion method with the presence of ionic platinum.

Beside the effect of weak CO bonding to ionic Pt, the CO tolerance of Pt-$CeO_2$ catalyst can be also enhanced due to CO oxidation by oxygen released form cerium oxide (oxygen storage capacity effect).

The origin of the peak P5 at 0.7 V obtained for Pt-$CeO_2$/GDL was not clear; however this peak might correspond to methanol decomposition to different products like formic acid or formaldehyde [20,28] which was supposed to be due the increased availability of Pt surface sites for methanol oxidation on the GDL by rapid desorption of bi-sulfate ions [36]. This structural difference (peak at 0.7V) of Pt/CeO2 on GDL and GF can also be seen by the comparison of cyclic voltammograms of GDL and GF supported Pt-CeO2 films after hydrogen bubbling, exhibiting significant hydrogen adsorption desorption peaks on the GDL substrate (see Fig. 5).

## 5. CONCLUSION

The cyclic voltammetric experiments on Pt-$CeO_2$ thin layer prepared by magnetron sputtering on GDL and carbon foil exhibited higher performance for hydrogen a methanol electro-oxidation compared to the commercial Pt-C nanopowder. The both catalysts have been found to be promising materials for methanol electro-oxidation since these layers exhibited high resistance to CO poisoning, which is most probably due to ionic states of $Pt^{n+}$ in the Pt-$CeO_2$ layers. In addition, the GDL and GF

substrates can affect the structure of Pt clusters and the ratio of $Pt^{+2}/Pt^{0}$ on the sputtered layer which was observed as a methanol oxidation peak at low voltage 0.7 V and distinguished hydrogen adsorption desorption peaks on Pt-$CeO_2$/GDL catalyst during cyclic voltammetry after hydrogen bubbling.

ACKNOWLEDGEMENTS

The research support was provided by The Grant Agency of Charles University, no. 388711, Czech Science Foundation under projects GACR P204/10/1169 and 13-10396S, and by the project LD13054 of the Czech Ministry of Education. K.S. thanks NIMS for the support NIMS covering her research stay at BL15XU beamline at the synchrotron Spring 8 in Japan.

## References

1. A. Katayama, *J. Phys. Chem*., 84 (1980) 376-381.
2. P. K. Shen and A. C. C. Tseung, *J. Electrochem. Soc*., 141 (1994) 3082-3090.
3. J. Rajeswari, B. Viswanathan and T. K. Varadarajan, *Mater. Chem. Phys*., 106 (2007) 168-174.
4. C. W. Xu, R. Zeng, P. K. Shen, and Z. D. Wei, *Electrochim. Acta*, 51 (2005) 1031-1035.
5. C. L. Campos, C. Roldan, M. Aponte, Y. Ishikawa and C. R. Cabrera, *J. Electroanal. Chem*., 581 (2005) 206-215.
6. M. Takahashi, T. Mori, F. Ye, A. Vinu, H. Kobayashi and J. Drennan, *J. Am. Ceram. Soc.*, 90 (2007) 1291-1294.
7. M. Vaclavu, I. Matolinova, J. Myslivecek, R. Fiala and V. Matolin, *J. Electrochem. Soc*., 156 (2009) B938-B942.
8. M. Vaclavu, I. Matolinova, J. Myslivecek, R. Fiala, VMatolin V. Matolin, M. Cabala, I. Matolinova, M. Skoda, M. Vaclavu, K. C. Prince, T. Skala, T. Mori, H. Yoshikawa, Y. Yamashita, S. Ueda and K. Kobayashi, *Fuel Cells*, 10 (2010) 139-144.
9. V. Matolin, I. Matolinova, M. Vaclavu, I. Khalakhan, M. Vorokhta, R. Fiala, I. Pis, Z. Sofer, J. Poltierova-Vejpravova, T. Mori, V. Potin, H. Yoshikawa, S. Ueda and K. Kobayashi, *Langmuir*, 26 (2010) 12824-12831.
10. P. Bera, K. C. Patil, V. Jayaram, G. N. Subbanna and M. S. Hedge, *J. Catal*., 196 (2000) 293-301.
11. P. Bera, A. Gayen, M. S. Hedge, N. P. Lalla, L. Spadaro, F. Frusteri and F. Arean, *J. Phys. Chem*. B, 107 (2003) 6122-6130.
12. A.E. Aksoylu, Z. I. Onsan, *Turk. J. Chem.*, 33(2009) 589.
13. G. Dutta, U. V. Waghmare and T. and Hedge M. S. Baidya, *Chem. Mater*., 19 (2007) 6430-6436.
14. R .Fiala, I. Khalakhan, I. Matolinova, M. Vaclavu, M. Vorokhta, Z. Sofer, S. Huber, V. Potin and V. Matolin, *J. Nanosci. Nanotechnol*., 11 (2011) 5062–5067.
15. S. Tanuma, C. J. Powell, D. R. Penn, *Surf. Interf. Anal*., 21 (1993), 165.
16. A. Fujimori, *Phys. Rev*. B, 28 (1983) 2281–2283.
17. V. Matolín, M. Cabala, V. Cháb, I. Matolínová, K. C. Škoda M Šutara F. Prince, T. Skála and K. Veltruská, *Surf. Interf. Ana*.l, 40 (2008) 225–230.
18. T. Skála, F. Šutara, K. C. Prince and V. Matolin, *J. Electron Spectrosc. Relat. Phenom*., 169 (2009) 20–25.
19. L. Osterlund, S. Kielbassa, C. Werdinius and B. Kasemo, *J. Catal*., 215 (2003) 94–107.
20. G. García, J. Florez-Montaño, A. Hernandez-Creus, E. Pastor and G. A. Planes, *J. power sources*, 196 (2011) 2979–2986.
21. P. Justin, P.H.K. Charan and R. G. Rao, *Appl. Catal. B-Envirnl*., 100 (2010) 510–515.

22. K. Fugane, T. Mori, D. R. Ou, A. Suyuki, H. Yoshikawa, T. Masuda, K. Uosaki, Y. Yamashita, S. Ueda, K. Kobayashi, N. Okazaki, I. Matolinova and V. Matolin, *Electrochim. Acta*, 56 (2011) 3874-3883.
23. G. Wu, L. Li and B.-Q. Xu, *Electrochim. Acta*, 50 (2004) 1-10.
24. C. Lee, H. Ojima and M. Umeda, *Electrochim. Acta*, 53 (2008) 3029-3035.
25. J. Macdonald, B. Gualtieri, N. Runga, E. Teliz and C. Zinola, *Int. J. Hydrogen Energy*, 33 (2008) 7048-7061.
26. M.A. Scibioh, S.-K. Kim, E.A. Cho, T-H. Lim, S.-A. Hong and H.Y. Ha, *Appl. Catal. B-Environ*., 84 (2008) 773–782.
27. S. Garbarino, A. Ponrouch, S. Pronovost and D. Guay, *Electrochem. Commun*., 11 (2009) 1449–1452.
28. P. Hernández-Fernández, R. Nuño, E. Fatás, J.L.G. Fierro and P. Ocón, *Int. J. Hydrogen Energ*., 36 (2011) 8267–8278.
29. S. Sharma, P. Singh and M.S. Hegde, *J. Solid State Electrochem*, 15 (2011) 2185-2197.
30. T. Iwasita, H. Hoster, A. John-Anacker, W. F. Lin and W. Vielstich, *Langmuir*, 16 (2000) 522-529.
31. M. Soszko, M. Łukaszewski, Z. Milanowska and A. Czerwinñski, *J. power sources*, 196 (2011) 3513–36522.
32. J.-F. Drillet, A.E.J. Friedemann, R. Kötz, B. Schnyder and V.M. Schmidt, *J. Mater. Chem*., 2 (1992) 875-887.
33. Z. Liu, X.Y. Ling, X. Su and J.Y. Lee, *J. Phys. Chem*. B., 108 (2004) 8234-8240.
34. J. Zhao, Ch. Weixiang and Y. Zheng, *Mater. Chem. phys*., 113 (2009) 591–595.
35. M.S.I. Dual, M.-S. Won and Y-B. Shim, *J. Alloy. Compd*., 494 (2010) 463–467.
36. H.F.Wang, Z.P.Liu, *J. Am. Chem. Soc*., 130 (2008) 10996-11004.